Absorption and Resonance Raman Study of the $^2B_1(X)-{}^2A_2(A)$ Transition of Chlorine Dioxide in the Gas Phase

Anthony P. Esposito, Todd Stedl, Hannes Jónsson, and Philip J. Reid*

Department of Chemistry, University of Washington, P.O. Box 351700, Seattle, Washington 98195

Kirk A. Peterson

Department of Chemistry, Washington State University, 2710 University Drive, Pullman, Washington 99164-4630

Received: November 9, 1998; In Final Form: January 27, 1999

The photochemical reaction dynamics of chlorine dioxide (OClO) are investigated using absorption and resonance Raman spectroscopy. The first Raman spectra of gaseous OClO obtained directly on resonance with the $^2B_1-{}^2A_2$ electronic transition are reported. Significant scattering intensity is observed for all vibrational degrees of freedom (the symmetric stretch, bend, and asymmetric stretch), demonstrating that structural evolution occurs along all three normal coordinates following photoexcitation. The experimentally measured absorption and resonance Raman intensities are compared to the intensities predicted using both empirical and ab initio models for the optically active $^2A_2$ surface. Comparison of the experimental and theoretical absorption spectra demonstrates that the frequencies and intensities of transitions involving the asymmetric stretch are well reproduced by the empirical model characterized by a double-minimum along the asymmetric stretch. However, the ab initio model is also found to reproduce a subset of the experimental intensities. In addition, the extremely large resonance Raman intensity of the asymmetric stretch overtone transition is predicted by both models. The results presented here taken in combination with the model for the $^2A_2$ surface in condensed environments suggest that the phase-dependent photochemical reactivity of OClO is due to environment-dependent excited-state structural evolution along the asymmetric stretch coordinate.

Introduction

The photochemistry of chlorine dioxide (OClO) is of current interest in atmospheric chemistry because of the participation of this compound in the reactive chlorine reservoir as well as its potential role in stratospheric ozone layer depletion.[1−5] Photoexcitation of OClO results in either the formation of ClO ($^2\Pi$) and O (^3P_g), or Cl (^2P_u) and O_2 ($^1\Delta_g$, $^3\Sigma_g$).[1,6−58] In addition, the Cl and O_2 products may be preceded by the formation of the peroxy isomer, ClOO, produced by the photoisomerization of OClO.[1,15,16,18,20,25,33,55] The intriguing aspect of this photochemistry is that the partitioning between product pathways is phase-dependent. For example, the quantum yield for Cl formation (Φ_{Cl}) is ∼0.04 in the gas phase,[10−14,37] but increases to near unity in low-temperature matrices and on surfaces.[33,40,41,49−54,59] Solutions represent an intermediate case with $\Phi_{Cl} \approx 0.1$ in water.[16,18,20−23,27,29,30] Elucidating the origin of this phase dependence is currently the central problem in OClO photochemistry.

Recent work regarding OClO photochemistry has demonstrated that the structural evolution on the optically prepared $^2A_2$ surface is intimately coupled to photoproduct formation.[21,28,32,56−58] In particular, evolution along the asymmetric stretch coordinate is believed to be critical in defining the photoproduct quantum yields. Two models for the $^2A_2$ potential energy surface along the asymmetric stretch coordinate in the gas phase have been proposed. Through analysis of the rotationally resolved electronic absorption spectrum of gaseous OClO, Richard and Vaida demonstrated that the unusually large intensity observed for transitions involving the asymmetric stretch can be reproduced by including an energy barrier along this coordinate (i.e., a double-minimum surface as depicted in Figure 1A).[7] In contrast, ab initio studies performed by Peterson and Werner suggested that the potential energy surface along the asymmetric stretch coordinate is roughly harmonic with appreciable anharmonic coupling to the symmetric stretch (Figure 1B).[56−58] We recently completed the resonance Raman intensity analysis of OClO in water and cyclohexane where the curvature of the $^2A_2$ surface in these solvents was determined.[28,31,32] We found that the $^2A_2$ surface along the asymmetric stretch is significantly different in these solvents relative to either model of the gas-phase potential energy surface (Figure 1C). Specifically, the limited resonance Raman intensity of the asymmetric stretch overtone transition was found to be consistent with a harmonic potential along this coordinate with $\omega_e \geq 750\ cm^{-1}$. In solution, limited structural evolution occurs along the asymmetric stretch; however, significant structural evolution along this coordinate is predicted by both gas-phase models. Given this difference in excited-state dynamics, we suggested that the increase in quantum yield for Cl formation in condensed environments originates from the preservation of C_{2v} symmetry on the optically prepared excited state.[28,32,57]

The photochemical model outlined above is consistent with all of the experimental and theoretical results presented to date; however, it relies on comparison of $^2A_2$ surface descriptions derived from various techniques (i.e., absorption, resonance

* To whom correspondence should be addressed. E-mail: preid@chem.washington.edu. Phone: (206) 528-1127.

10.1021/jp984368i CCC: $18.00
Published on Web 03/09/1999

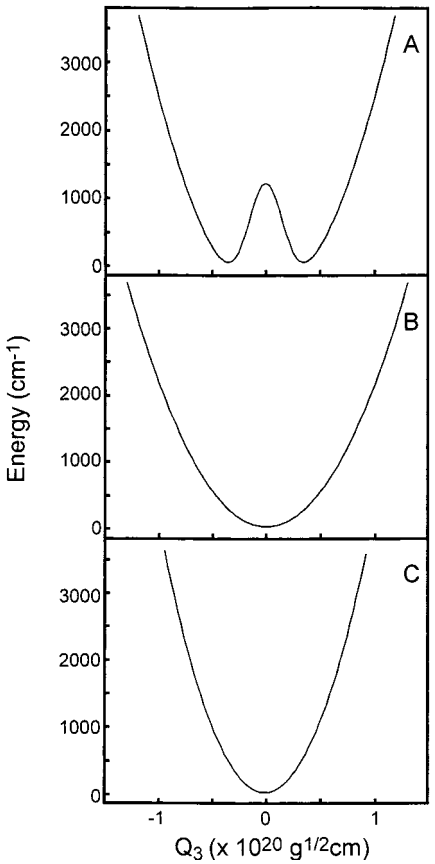

Figure 1. Current models for the optically prepared $^2A_2$ potential energy surface along the asymmetric stretch coordinate: (A) Potential energy surface determined by analysis of the gas-phase absorption spectrum;[7] (B) potential energy surface determined by ab initio theoretical analysis;[56−58] (C) potential energy surface determined by resonance Raman intensity analysis of OClO in water and cyclohexane.[28,32]

Raman, and ab initio theory). It has been appreciated for some time that absorption and resonance Raman are complementary, since both depend on the displacement and curvature of the optically active excited state.[60−62] Therefore, direct comparison of the potential-energy-surface parameters derived from these techniques is not without merit; however, it has yet to be demonstrated that the resonance Raman intensities of gas-phase OClO are consistent with either model. In addition, a quantitative comparison of the absorption or resonance Raman intensities predicted by the ab initio model to the experimental spectra has not been performed to date. Finally, the ab initio results have created some ambiguity concerning the presence of an excited-state barrier along the asymmetric stretch. The work presented here was performed to address these issues.

In this paper, we present an analysis of the absorption and resonance Raman intensities of gaseous OClO. We present the first Raman spectrum of gaseous OClO obtained directly on resonance with the $^2B_1-{}^2A_2$ transition. Raman transitions involving both the symmetric stretch and bend coordinates are observed, demonstrating that the excited-state structural evolution is characterized by motion along these coordinates. Most interesting is the extremely large intensity observed for the asymmetric stretch overtone transition. The substantial intensity of this transition demonstrates that in the gas phase, significant excited-state structural evolution also occurs along this coordinate following photoexcitation. A theoretical analysis of the absorption and resonance Raman intensities is performed where the experimental intensities are compared to intensities predicted using both the double-minimum and ab initio models for the $^2A_2$ surface. The substantial intensity of transitions involving the asymmetric stretch in both the absorption and resonance Raman spectra is found to be adequately reproduced by both models. This result demonstrates that for gas-phase OClO, significant structural evolution along the asymmetric stretch coordinate occurs following photoexcitation. This result combined with our earlier work in condensed environments supports the hypothesis that differences in evolution along the asymmetric stretch coordinate are responsible for the phase-dependent photochemistry of OClO.

Experimental Methods

Materials. Gaseous OClO was synthesized as previously described.[32] The samples used in this study were produced by bubbling gaseous OClO through either cyclohexane or hexanes (Fisher, HPLC grade) until a concentration of ∼30 mM was reached as determined by static vis−UV absorption. OClO was then removed from solution by passing a carrier gas though this solution as described below. It should be noted that extreme care must be taken in the preparation and handling of gaseous OClO in that it can (and unfortunately will) explode at pressures above 30 Torr.

Absorption Spectra. Absorption spectra were measured on a Varian Cary 219 scanning spectrometer with an experimental resolution of ∼10 cm^{-1}. The absorption spectrum was acquired by placing a small volume of the sample at the bottom of a closed quartz cuvette such that the spectrum of OClO vapor at ambient temperature (∼293 K) was recorded. Repeated scanning of the absorption spectrum was performed to ensure that photolysis of gaseous OClO did not significantly perturb the measured intensities. Absorption cross sections were taken from previously reported values.[63]

Resonance Raman Spectra. Excitation wavelengths of 368.9 and 360.3 nm were obtained by stimulated Raman shifting the second-harmonic output of a Nd:YAG laser (Spectra Physics, GCR-170) in H_2 or D_2, respectively. The incident light was focused onto the sample using a 100 mm focal length plano-convex UV-quality spherical lens. A 90° scattering geometry was employed with the scattered light collected and delivered to a 0.75 m spectrograph (Acton) using standard, refractive UV-quality lenses. The scattered light passed through a polarization scrambler located at the spectrograph entrance and was dispersed by either a 300 groove/mm (classically ruled), a 1200 groove/mm (classically ruled), or a 2400 groove/mm (holographic) grating. Detection of the scattered light was accomplished using an 1100 × 330 pixel, back-thinned, liquid-nitrogen-cooled CCD detector (Princeton Instruments). Spectrometer slit widths were adjusted to provide a spectral resolution of 10 cm^{-1}. Calibration of the Raman spectra was accomplished by reference to the methane carrier gas transition at 2917 cm^{-1} as well as the emission from Ne, Fe, and Hg standard lamps. All spectra were corrected for the wavelength-dependent sensitivity of the spectrometer using either calibrated D_2 (Hellma) or quartz−tungsten−halogen (Oriel) lamps. The spectra are uncorrected for self-absorption.

Chlorine dioxide was degassed from solution by passing a 12 psi stream of methane through a 250 mL reservoir containing the OClO/solvent sample described above. The OClO/methane stream was delivered to the spectrometer via Teflon lined Tygon tubing connected to a quartz pipet having an exit aperture diameter of 1.5 mm. The excitation beam intersected the gas stream approximately 2 mm from the pipet end. The entire pipet

assembly was surrounded by a square-walled quartz tube connected to a vacuum line providing for gas collection and disposal. The OClO concentration in the sample reservoir was monitored at the start and end of a given experiment. For experiments where a single spectral frame was collected, the OClO reservoir concentration was allowed to decrease by 50% before termination of the experiment. For experiments where adjacent spectral frames were collected, a reduction in concentration of up to 30% for a single frame was allowed before replacing the reservoir and acquiring the next frame. Although the change in concentration is substantial, adjacent spectral frames contained a common OClO Raman transition such that the frames could be scaled before combining. In addition, spectra obtained when spectral frames were collected with different orderings were identical. The OClO scattering observed at 368.9 nm was found to be linear for pulse energies up to ~50 μJ. Therefore, pulse energies of 33 μJ were employed in this study and adjusted at 360.3 nm with reference to the absorption cross section at this wavelength relative to 368.9 nm to ensure minimal sample photoalteration.

Computational Methods

Absorption and Resonance Raman Cross Sections. Calculation of the absorption (σ_A) and Raman (σ_R) cross sections was performed employing the time-dependent formalism of Heller and co-workers where the cross sections are given by[60−62,64,65]

$$\sigma_A(E_1) = \frac{4\pi e^2 E_1 M_{eg}^2}{6\hbar^2 cn}\int_{-\infty}^{\infty}\langle i|i(t)\rangle \exp[i(E_1 + E_i)t/\hbar]\exp\left(\frac{-\Gamma|t|}{\hbar}\right)dt \quad (1)$$

$$\sigma_R(E_1) = \frac{8\pi E_s^3 E_1 e^4 M_{eg}^4}{9\hbar^6 c^4}\left|\int_0^{\infty}\langle f|i(t)\rangle \exp[i(E_1 + E_i)t/\hbar]\exp\left(\frac{-\Gamma t}{\hbar}\right)dt\right|^2 \quad (2)$$

where M_{eg} is the transition moment of the photochemically relevant transition, E_l is the energy of the incident radiation, E_s is the energy of the scattered light, E_i is the energy of the initial vibrational state, and n is the index of refraction (taken to be that of air). The homogeneous line width (represented by Γ) is modeled as Lorentzian. The $\langle i|i(t)\rangle$ term in eq 1 represents the time-dependent overlap of the initial state, and this same state propagating under the influence of the excited-state Hamiltonian (i.e., the absorption time-correlator). The $\langle f|i(t)\rangle$ term in eq 2 (i.e., the Raman time-correlator) is also a time-dependent overlap term where $|f\rangle$ is the final state in the scattering process.

Equations 1 and 2 are correct in the limit where the absorption or resonance Raman spectrum is vibronic; however, rotational dynamics are of relevance in these experiments. Therefore, the influence of rotations on the absorption cross section was explored as follows. OClO is formally an asymmetric rotor (rotational constants are presented in Table 1);[44] however, the asymmetry parameter is −0.92 such that OClO can be approximated as a prolate symmetric top.[66−69] In applying this approximation, we retain the A rotational constants reported in Table 1 and average the B and C rotational constants, resulting in approximate minor rotational constants of $C_g = 0.305$ cm^{-1} and $C_e = 0.276$ cm^{-1} (where g and e refer to the ground and excited electronic states, respectively). The angular momentum coupling of OClO conforms to Hund's second case such that the total angular momentum is defined as $J = N + S$ where S is the total spin ($\pm^1/_2$).[8,68,69] The spectral resolution of these experiments is insufficient to observe band splitting due to spin; therefore, these contributions are ignored. With the above approximations, and invoking rovibronic separability and the Born−Oppenheimer approximation, the absorption cross section can be written as[70,71]

TABLE 1: Rotational Constants of OClO

rotational constant (cm^{-1})	$^2B_1$(X)	$^2A_2$(A)
A	1.737	1.057
B	0.332	0.311
C	0.278	0.240
C_{approx}[a]	0.305	0.276

[a] Approximate rotational constant employed in prolate-symmetric-top limit. This value is obtained by taking the average value of the two minor rotational constants.[44]

$$\sigma_A \propto M_{eg}^2 \sum_v |\langle v|i\rangle|^2 \sum_{NK} P_{NK} \times \sum_{N'K'M'} \frac{|\langle N'K'M'|C_{az}|NKM\rangle|^2}{(E_{vi} + E_{N'K'NK} - E_l)^2 + (\Gamma_{vN'K'M'} + \eta)^2} \quad (3)$$

where v and $N'K'$ are the excited vibrational and rotational states, respectively, and i and NK denote the initial vibrational and rotational states, respectively. $\langle N'K'M'|C_{az}|NKM\rangle$ are the directional cosine matrix elements for a parallel-type transition. The selection rules for transitions of this type are[68]

$$K = 0 \qquad \Delta K = 0, \quad \Delta N = \pm 1 \quad (4a)$$

$$K \neq 0 \qquad \Delta K = 0, \quad \Delta N = 0, \pm 1 \quad (4b)$$

Given the magnitude of the rotational constants (Table 1) and the temperature at which the experiments were performed, the high-N limit is applicable where $(N + 1) \approx (N + 3) \approx N$. In this limit, summation over the M-state manifold results in the following expressions for the directional cosine matrix elements:

$$|\langle NKM|C_{az}|NKM\rangle|^2 = \frac{2K^2}{3N} \quad (5a)$$

$$|\langle (N-1)KM|C_{az}|(N-1)KM\rangle|^2 = \frac{N^2 - K^2}{3N} \quad (5b)$$

$$|\langle (N+1)KM|C_{az}|(N+1)KM\rangle|^2 = \frac{N^2 - K^2}{3N} \quad (5c)$$

In eq 3, P_{NK} is the probability of occupying the initial rotational state $|NK\rangle$. For OClO, the ^{16}O nuclei conform to Bose−Einstein statistics. Employing the I^r representation, the symmetry axis is assigned x orientation, orthogonal to the unique moment of inertia (z orientation).[69] The overall wave function must be symmetric with respect to C_2 rotation about the symmetry axis, and the rotational wave functions are even or odd with respect to N; therefore, odd and even N states are populated in the B_1 ground and A_2 excited states, respectively. E_{vi} is the energy difference between the ground and excited vibronic states, E_l is the energy of the incident radiation, and $E_{N'K'NK}$ is the energy difference between the excited and ground rotational states given by[66]

$$E_{N'K'NK} = C_e N'(N'+1) - C_g N(N+1) + [(A_e - A_g) - (C_e - C_g)]K^2 \quad (6)$$

Also in eq 3, $\Gamma_{\upsilon N'K'M'}$ is the homogeneous line width and η is the line width introduced by the instrument response (also modeled as Lorentzian). Equation 3 demonstrates that at this level of approximation, the absorption spectrum can be thought of as a series of transitions whose intensities are dependent on the Franck−Condon factors between a given initial and final vibrational level. These transitions are then multiplied by the rotational transition probability resulting in the observed intensities. The Franck−Condon factors were determined by performing the calculation prescribed by eq 1 (without scaling for excitation wavelength) and measuring the calculated vibronic transition amplitudes. Calculation of the absorption spectrum was then accomplished by using these Franck−Condon factors in performing the summation over the rovibronic manifold as prescribed by eq 3. The resonance Raman cross section calculations are performed without including rotations. We are currently extending the theory presented here to include rotations, and a report employing this extended theory to model the gas-phase resonance Raman cross sections of OClO will appear shortly. Although the calculated Raman intensities can only be qualitatively compared to the experimental results presented below, the analysis performed here does provide insight into the substantial differences in predicted Raman intensity between the double-minimum and ab initio surfaces.

Ground and Excited Potential Energy Surfaces. To evaluate eqs 1 and 2, it is necessary to calculate the time-dependent overlap factors $\langle i|i(t)\rangle$ and $\langle f|i(t)\rangle$, with these terms being dependent on the model employed for the ground and excited-state potential energy surfaces. In the calculations performed using the double-minimum model, all three normal coordinates were modeled as harmonic in the ground state (Table 2), whereas the $^2B_1$ ab initio wave functions were used in the ab initio calculations. The lowest frequency mode of OClO is at 450 cm^{-1}; therefore, the initial state was taken to be the ground vibrational state along all coordinates (i.e., the 0 K approximation is assumed to be valid).

Two models for the optically active $^2A_2$ excited state were employed. First, a double-minimum potential similar to that of Richard and Vaida was investigated.[7] This potential can be expressed as

$$V_e = \frac{1}{2}\frac{\omega_{e1}^2}{\omega_{g1}}(q_1-\Delta_1)^2 + \frac{1}{2}\frac{\omega_{e2}^2}{\omega_{g2}}(q_2-\Delta_2)^2 + \frac{1}{2}\frac{\omega_{e3}^2}{\omega_{g3}}(q_3)^2 + \frac{1}{6}\chi_{111}\left(\frac{\omega_{e1}}{\omega_{g1}}\right)^{3/2}(q_1-\Delta_1)^3 + A\exp\left(-a^2 q_3^2\frac{\omega_{e3}}{\omega_{g3}}\right) \quad (7)$$

where ω_g and ω_e are the ground and excited-state frequencies along the symmetric stretch, bend, and asymmetric stretch (denoted by the subscripts 1, 2, and 3, respectively). The first three terms in eq 7 represent the harmonic contributions to the potential. Displacement of the excited-state potential energy surface minimum relative to the ground state along each coordinate is denoted as Δ, with displacement incorporated only for the bend and symmetric stretch degrees of freedom, since these modes are totally symmetric. Cubic anharmonicity along the symmetric stretch coordinate is included through the term containing χ_{111}. Anharmonic coupling between coordinates is not included such that each degree of freedom can be modeled as separable. With separability, the multidimensional absorption and Raman time-correlators can be decomposed into a product of one-dimensional overlaps. The overlap along the bend was calculated using the analytic expressions of Mukamel and coworkers.[72] Overlaps along the symmetric and asymmetric stretch were determined using the approximate method of Feit and Fleck where[73,74]

$$|i(\Delta t)\rangle = \exp(i\hbar(\Delta t)\nabla^2/(4M))\exp(-i(\Delta t)V_e/\hbar)\times \exp(i\hbar(\Delta t)\nabla^2/(4M))|i(0)\rangle + \vartheta(\Delta t^3) \quad (8)$$

In eq 8, ∇^2 is the Laplacian in position space, V_e is the excited-state potential, and Δt is the propagation time step. For gaseous OClO, the structure in the absorption spectrum demonstrates that the homogeneous line width is modest; therefore, the time-dependent overlaps must be calculated for relatively long times compared to other systems in which substantial homogeneous broadening limits the necessary time for propagation. Given this constraint, a time step of 0.1 fs was employed with 30 000 time steps calculated per overlap. Reductions in the step size and/or an increase in the number of time steps taken did not alter the results presented here. The specific parameters employed in evaluating eq 7 are presented in Table 2A.

TABLE 2: Parameters Used in the Double-Minimum and ab Initio Representations of the $^2A_2$ Surface

	mode[a]	ω_g (cm^{-1})[b]	ω_e (cm^{-1})[b]	Δ[c]
	(A) Double Minimum			
	ν_1[d]	945	700	5.7
	ν_2	450	270	0.6
$E_{00} = 17\,937$ cm^{-1}	ν_3[e]	1100	455	0
	(B) Ab Initio[f]			
	ν_1	960.15	720.43	4.345
	ν_2	455.62	288.09	−1.645
$E_{00} = 21\,045$ cm^{-1}	ν_3	1127.82	419.20	0

[a] Subscripts 1, 2, and 3 refer to the symmetric stretch, bend, and asymmetric stretch, respectively. [b] The symbols ω_g and ω_e refer to the ground- and excited-state harmonic frequencies, respectively. [c] Dimensionless displacement of the excited-state potential energy surface minimum relative to that of the ground state along a given coordinate. [d] Calculation employed -90 cm^{-1} for χ_{111}, the anharmonicity prefactor for the cubic term in the series expansion of the potential energy surface (eq 7). [e] Potential along this coordinate was modeled as harmonic, with a Gaussian barrier ($A = 1673$ cm^{-1} and $a = 2.4$) centered at $q_3 = 0$, as described in the text (eq 7). [f] Values correspond to the normal-coordinate description of the $^2A_2$ surface.

The second model employed for the $^2A_2$ surface was the ab initio potential of Peterson.[56] The three-dimensional potential energy functions (PEFs) describing the ground and excited states of OClO were fit to polynomials employing an internal coordinate description defined by the authors. To facilitate comparison to the double-minimum model, we transformed the PEFs into normal coordinates as follows. The equilibrium geometry of the molecule was defined with the center of mass located at the origin and the Cl atom positioned along the negative y axis. This definition allowed for nonlinear determination of the exact Cartesian coordinate displacements involving each atom in the internal coordinate representation and also provides for facile fitting of the PEFs in terms of the two, in-plane Cartesian displacements of each atom. The corresponding 6-by-6 mass-weighted force matrix (**f**) describing the $^2B_1$ ground state was defined using standard, normal-coordinate techniques.[75] The **f** matrix was then diagonalized in order to generate the normal modes through

$$\mathbf{f}L = L\Lambda \quad (9)$$

where the L matrix contains the eigenvectors and Λ is a diagonal matrix containing the eigenvalues (λ_k). Vibrational frequencies for a given normal mode are related to the eigenvalues by

$$\lambda_k = \left(\frac{\omega_k}{\hbar}\right)^2 \tag{10}$$

The portion of the L matrix corresponding to vibrations was used to define the normal coordinates q through

$$L_q = \mathbf{M}^{-1/2} L \zeta^{-1} \tag{11}$$

were **M** is a 6-by-6 diagonal matrix containing the atomic masses and ζ is a 3-by-3 diagonal matrix with elements

$$\zeta_k = \frac{\sqrt{\omega_k}}{\hbar} \tag{12}$$

The elements of L_q define the relationship between normal coordinates and Cartesian displacements:

$$\begin{bmatrix} \delta x_{\mathrm{Cl}} \\ \delta y_{\mathrm{Cl}} \\ \delta x_{\mathrm{O+}} \\ \delta y_{\mathrm{O+}} \\ \delta x_{\mathrm{O-}} \\ \delta y_{\mathrm{O-}} \end{bmatrix} = L_q \begin{bmatrix} q_1 \\ q_2 \\ q_3 \end{bmatrix} =$$

$$\begin{bmatrix} 0 & 0 & -0.0185169 \\ -0.0155116 & 0.0224488 & 0 \\ 0.0233913 & 0.0340610 & 0.0202412 \\ 0.0169561 & -0.0245393 & 0.0122465 \\ -0.0233913 & -0.0340610 & 0.0202412 \\ 0.0169561 & -0.0245393 & -0.0122465 \end{bmatrix} \begin{bmatrix} q_1 \\ q_2 \\ q_3 \end{bmatrix} \tag{13}$$

The elements of L_q have units of angstroms, and the subscripts 1, 2, and 3 corresponding to the symmetric stretch, bend, and asymmetric stretch normal modes, respectively.

The approach outlined above allows the $^2A_2$ PEF originally defined in terms of internal coordinates to be defined in terms of a three-dimensional normal coordinate grid for use in the calculation of the absorption and Raman time-correlators. Specifically, for each point on the PEF grid, normal coordinates were used to find the corresponding atomic Cartesian displacements via eq 13. The Cartesian displacements were then used to determine the grid location in internal coordinates. Finally, the internal-coordinate locations were used to define the energy of the PEF. By use of this methodology, the full, three-dimensional ab initio surface in the normal coordinate basis was determined.

To simplify comparison of the ab initio and double-minimum models, the L_q matrix was also used to determine the displacements of the $^2A_2$ potential-energy-surface minima relative to the ground state. This was accomplished by taking the $^2A_2$ equilibrium configuration, determining the Cartesian displacements of this geometry relative to the ground-state equilibrium geometry, and transforming these displacements into normal coordinates using L_q as follows:

$$\begin{bmatrix} q_1 \\ q_2 \\ q_3 \end{bmatrix} = L_q^{-1} \begin{bmatrix} \delta x_{\mathrm{Cl}} \\ \delta y_{\mathrm{Cl}} \\ \delta x_{\mathrm{O+}} \\ \delta y_{\mathrm{O+}} \\ \delta x_{\mathrm{O-}} \\ \delta y_{\mathrm{O-}} \end{bmatrix} \tag{14}$$

The ground-state frequencies, excited-state frequencies, and excited-state displacements of the ab initio PEF described in the normal coordinate basis set are presented in Table 2B. It should be noted that the displacements determined here are in excellent agreement with a similar analysis of an earlier version of the ab initio surface.[22]

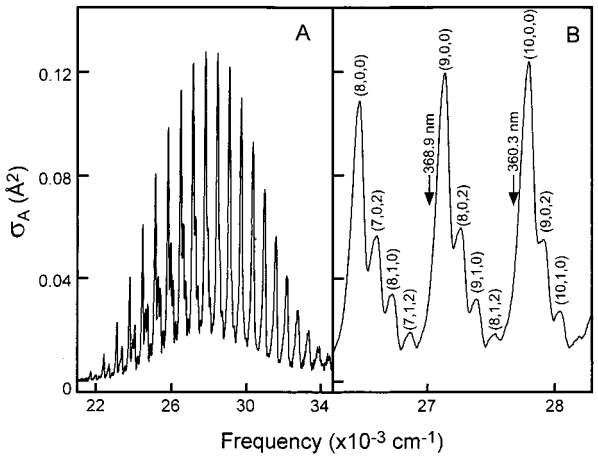

Figure 2. (A) Electronic absorption spectrum of chlorine dioxide vapor. Spectra were obtained at 293 K. Cross sections are taken from the literature.[63] (B) Expanded view of the absorption spectrum in the region studied by resonance Raman. The excitation wavelengths employed in the Raman study are shown. In addition, assignment of the transitions is presented as (n_1, n_2, n_3) where n is the number of quanta in the excited state along the symmetric stretch (1), bend (2), and asymmetric stretch (3) coordinates.

Given the description of the ab initio $^2A_2$ surface in normal coordinates, the time-dependent overlaps (eqs 1 and 2) were determined using a kinetic-referenced, three-dimensional version of the Feit and Fleck approximate propagation algorithm:[76]

$$|i(\Delta t)\rangle = \exp(-\mathrm{i}(\Delta t)V/(2\hbar)) \exp((-\mathrm{i}(\Delta t)/(2\hbar))\sum_k \omega_k p_k^2) \times \exp(-\mathrm{i}(\Delta t)V/(2\hbar))|i(0)\rangle + \vartheta(\Delta t^3) \tag{15}$$

where V is the $^2A_2$ PEF defined in normal coordinates, ω_k are the ground-state normal-mode frequencies, and p_k are the momenta in normal coordinates. The calculations were performed using a time step of 0.4 fs for a total of 20 000 time steps.

Experimental Results

Absorption. Figure 2A presents the absorption spectrum of OClO vapor obtained at ambient laboratory conditions. An expanded view of the region investigated in the resonance Raman study is presented in Figure 2B. The absorption spectrum is dominated by progressions involving the symmetric stretch coordinate (labeled (n, 0, 0) in Figure 2B).[7] In addition, transitions involving both the bend and symmetric stretch are observed (e.g., (8, 1, 0)). However, it is the large intensity of transitions involving the asymmetric stretch (e.g., (8, 0, 2)) that is the most interesting feature of the absorption spectrum. The ground-state symmetry of OClO is C_{2v} such that the asymmetric stretch coordinate is nontotally symmetric. Transitions involving odd quanta along the asymmetric stretch are not allowed by symmetry; however, even-quanta transitions may observed if the excited- and ground-state potential energy surfaces are significantly different.[7] The unusually large intensity of transitions involving the asymmetric stretch demonstrates that a substantial difference between the ground- and excited-state potential energy surfaces exists along this coordinate.

Resonance Raman. Resonance Raman spectra of gaseous OClO obtained with excitation at 368.9 and 360.3 nm are

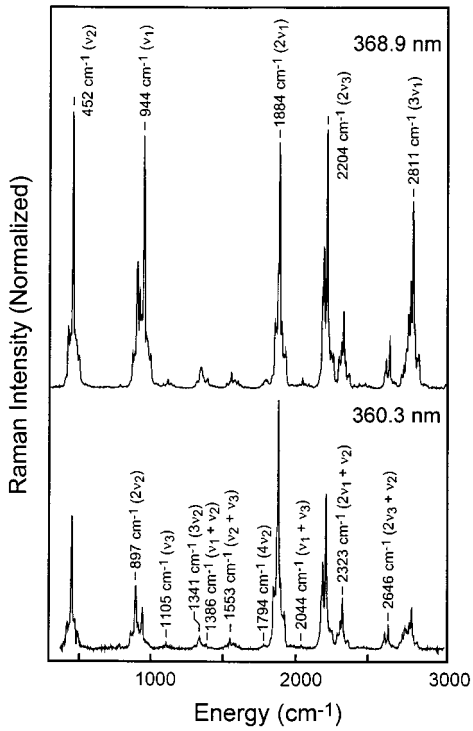

Figure 3. Resonance Raman spectra of gas-phase chlorine dioxide obtained with excitation wavelengths of 368.9 nm (top) and 360.3 nm (bottom). Frequencies and assignments for the observed transitions are given. Note the substantial intensity at both excitation wavelengths for the asymmetric stretch overtone transition ($2\nu_3$). Scattering from the methane carrier gas at 2917 cm^{-1} has been subtracted.

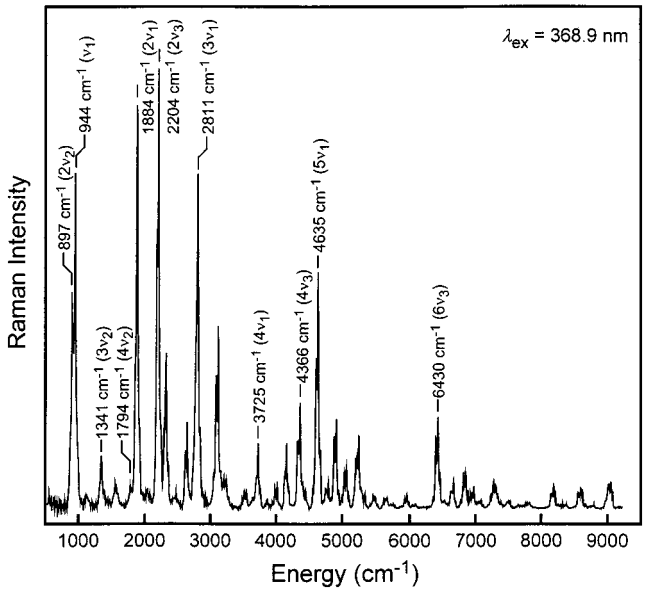

Figure 4. Resonance Raman spectrum of gas-phase chlorine dioxide obtained with 368.9 nm excitation. Fundamental and overtone transitions for all three normal coordinates are indicated.

presented in Figure 3. First, it is necessary to discuss whether the emission being observed is resonance Raman or resonance fluorescence. Elegant experimental work by Ziegler and coworkers has demonstrated that differentiation between emission types is dependent on the time scale for pure dephasing relative to population decay.[77] For the transitions investigated here (Figure 2B), the excited-state lifetimes are ≤ 1 ps. At the pressures employed in this study, the collisional frequency is ~ 0.01 ps^{-1} such that collisionally induced pure dephasing is much slower than population decay. An accurate measurement of the line width of the hydrogen- and deuterium-shifted Nd:YAG output could not be performed with our spectrometer; however, deconvolution provides a line width estimate of <1 cm^{-1}, suggesting that the coherence time of the excitation field is greater than the excited-state population decay time. Since pure dephasing is a prerequisite for fluorescence, the resonant secondary emission observed in this study is considered resonance Raman. This conclusion is supported by the observation that the transitions observed in the emission spectra track with excitation energy. In addition, the line widths for the Q-branch transitions observed in Figure 3 are ~ 2 cm^{-1} after deconvolution, much narrower than the line width expected if the emission occurs from an excited vibronic state having a ~ 1 ps decay rate.

The resonance Raman spectra presented in Figure 3 are dominated by transitions involving the symmetric stretch with fundamental (944 cm^{-1}) and overtone (1884 and 2811 cm^{-1}) transitions readily apparent. The direction of the $^2B_1-^2A_2$ transition dipole moment is parallel to the dominant rotational axis (i.e., a parallel-type transition); therefore, the absorption and Raman transitions are expected to be dominated by Q-branch activity, consistent with experiment.[7,55,78] In addition to the symmetric stretch, the bend also demonstrates significant intensity as evidenced by the large fundamental (452 cm^{-1}) and overtone (897 cm^{-1}) intensities corresponding to this coordinate. Numerous combination bands involving the symmetric stretch and bend are also observed. The most interesting pattern of scattered intensity involves the asymmetric stretch. In particular, the intensity in the asymmetric stretch overtone transition (2204 cm^{-1}) is extremely large. Small but measurable intensity is also observed for the asymmetric stretch fundamental transition (1105 cm^{-1}). The asymmetric stretch coordinate is nontotally symmetric such that fundamental resonance Raman intensity is not allowed by symmetry; however, even-overtone transitions involving this coordinate are allowed if there is a change in the curvature of the excited-state potential energy surface relative to the ground state.[79] The observation of overtone intensity along the asymmetric stretch coordinate demonstrates that the curvatures of excited and ground states along the asymmetric stretch coordinate are significantly different. In addition, the observation of a very weak asymmetric stretch fundamental intensity suggests that the excited-state potential energy surface is not absolutely symmetric about $Q_3 = 0$, potentially due to anharmonic coupling of the asymmetric stretch to other coordinates (see below).

Figure 4 presents an extended view of the resonance Raman spectrum of gaseous OClO obtained with 368.9 nm excitation. The fundamental and overtone transitions for the symmetric stretch, bend, and asymmetric stretch are indicated. Scattering is observed past 9000 cm^{-1} in contrast to the more limited range of observed intensity seen in the resonance Raman spectra of OClO in solution,[28,32] consistent with a reduction in the homogeneous line width in the gas phase.[62] The frequencies of the overtone transitions can be used to determine the curvature of the ground-state potential energy surface. The overtone transition frequencies and assignments for transitions involving the symmetric stretch are presented in Table 3. Assuming that the $^2B_1$ surface along the symmetric stretch is well described by a Morse potential, the anharmonicity along this coordinate can be determined by fitting the observed fundamental and overtone frequencies to the following expression:

$$\nu_n = n\omega_1 - n(n+1)\chi_{11} \qquad (16)$$

TABLE 3: Symmetric Stretch Fundamental and Overtone Raman Transitions of OClO

transition[a]	frequency (cm^{-1})[b]	frequency/n (cm^{-1})
ν_1	944 ± 2 (942 ± 1)	
$2\nu_1$	1884 ± 2 (1877 ± 1)	942 (938.5)
$3\nu_1$	2811 ± 3 (2804 ± 2)	937 (934.7)
$4\nu_1$	3725 ± 4 (3727 ± 2)	931.3 (931.8)
$5\nu_1$	4635 ± 5 (4624 ± 4)	927 (924.8)

[a] Prefactor indicates number of quanta exchanged between the symmetric stretch coordinate and the incident field. [b] First set of frequencies are those determined in this study. Frequencies in parentheses correspond to those reported for OClO isolated in cryogenic noble-gas matrices.[81]

where ν_n is the observed fundamental ($n = 1$) or overtone ($n > 1$) frequency, ω_1 is the frequency of the symmetric stretch in the harmonic limit, and χ_{11} is the anharmonicity.[80] Best fit of eq 16 to the fundamental and overtone frequencies resulted in $\omega_1 = 955 \pm 2$ cm^{-1} and $\chi_{11} = 4.82 \pm 0.4$ cm^{-1}, with $R = 0.9999$. These values are in excellent agreement with both ab initio theoretical results as well as the anharmonicity determined from analysis of preresonance Raman and resonance fluorescence spectra of OClO trapped in cryogenic noble-gas matrices.[24,56,81]

Computational Results

Absorption. The large intensities for transitions involving the asymmetric-stretch coordinate observed in both the absorption and resonance Raman spectra are consistent with significant excited-state structural evolution along this coordinate upon photoexcitation. Both gas-phase models for the $^2A_2$ potential-energy surface (Figure 1) are consistent with significant evolution along this coordinate; however, they differ with respect to the details of this evolution.[7,56] These differences can be investigated by comparing the absorption spectra predicted using these potentials to the experimental results.

First, the extent to which rotational dynamics are expected to contribute to the observed spectra must be addressed. Figure 5 demonstrates that individual rovibronic transitions are not expected to be evident because of the elevated temperature and finite resolution employed in these experiments. Figure 5A presents the rotational line width calculated for OClO in the prolate symmetric top limit at 40 K for a single vibronic transition. This spectrum was calculated using a Lorentzian line width of 0.25 cm^{-1}, similar to the line widths measured for rotationally cooled OClO.[8] Under these conditions, individual transitions are clearly observed. Figure 5B presents the 40 K rotational spectrum calculated using a Lorentzian line width of 10 cm^{-1} (i.e., the experimental resolution of our studies). This figure demonstrates that the effect of finite instrumental resolution is to eliminate the appearance of individual rotational transitions. Finally, Figure 5C presents the rotational spectrum calculated at 300 K with a Lorentzian line width of 10 cm^{-1}, demonstrating that at the elevated temperatures and finite resolution employed here, a broad rotational line width that extends asymmetrically to lower frequencies is expected.

Figure 6A presents a comparison of the experimental absorption spectrum to the calculated spectrum using the double-minimum model for the $^2A_2$ potential-energy surface (eq 7). Figure 6B presents the vibronic component of the calculated absorption spectrum (i.e., rotational line width is not included). Reproduction of the broadening evident in the spectra necessitated the addition of 15 cm^{-1} of homogeneous broadening in combination with the experimental line width of 10 cm^{-1}. This line width is substantially larger than the homogeneous broadening determined by analysis of the rotationally resolved absorption spectrum.[8] However, differences in experimental conditions combined with the population of higher rotational states at the temperature investigated here could result in an increase in the homogeneous line width. The figure demonstrates that the agreement between the experimental and calculated intensities using the double-minimum model is quite good. In particular, the model reproduces the relative intensities of the (n, 0, 0) and (n, 0, 2) transitions. This was the spectroscopic diagnostic employed by Richard and Vaida to justify the double-minimum model.[7] Figure 6C presents a comparison of the experimental absorption spectrum to the spectrum calculated using the ab initio potential energy surface, and Figure 6D presents the vibronic component of the calculated spectrum. The figures demonstrate that the ab initio surface adequately reproduces the relative intensities of the (n, 0, 0) and (n, 0, 2) transitions. However, the intensity of the progressions involving the symmetric stretch are not reproduced, suggesting that the displacement of the excited-state potential-energy-surface minimum relative to the ground state along this coordinate, or the anharmonicity along this coordinate, is not accurately reproduced by theory. It should also be noted that the ab initio data used in these calculations just extend into the Franck−Condon region of the $^2A_2$ surface; therefore, the discrepancy between the predicted and experimental intensities may reflect this limitation. The comparison of the experimental and theoretical absorption spectra presented here support the ability of the double-minimum model to reproduce the absorption spectrum of OClO in this spectral region; however, many of the major features of the absorption spectrum are reproduced by the ab initio model as well.

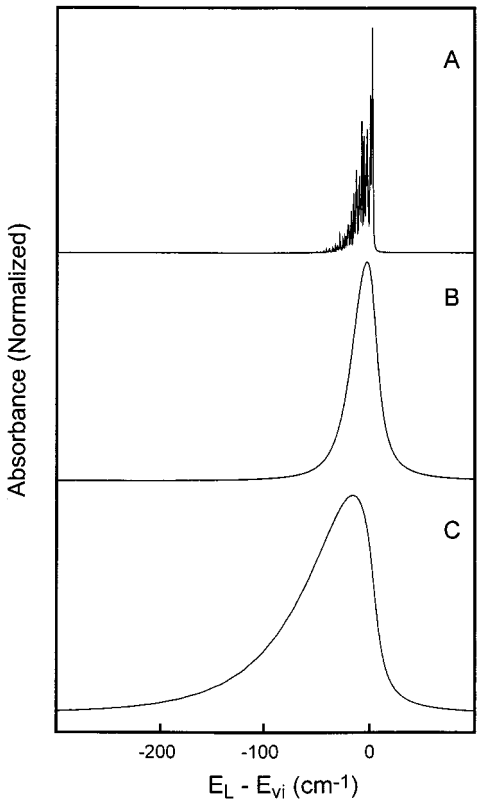

Figure 5. (A) Calculated absorption band for a single vibronic transition of OClO at 40 K employing a homogeneous line width of 0.25 cm^{-1}. (B) Calculated absorption band at 40 K employing a homogeneous line width of 10 cm^{-1}. (C) Calculated absorption band at 300 K employing a homogeneous line width of 10 cm^{-1}. Calculations were performed in the prolate-symmetric-top limit as discussed in the text.

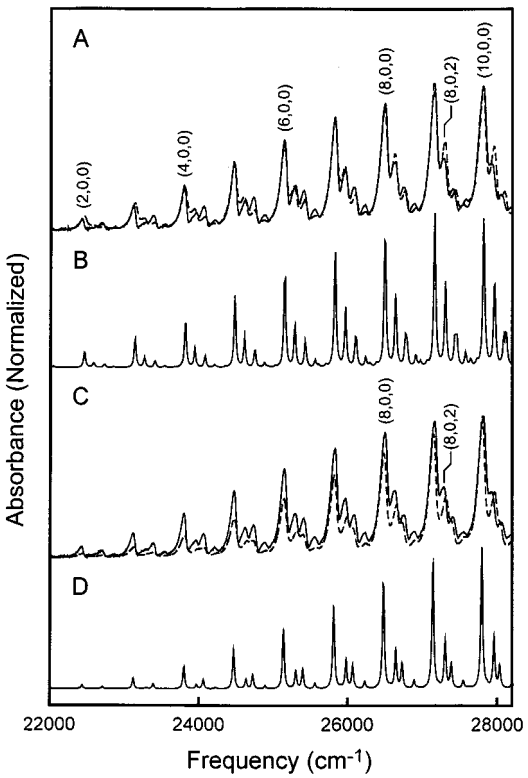

Figure 6. (A) Comparison of the experimental absorption spectrum (solid line) to that calculated employing a double-well potential along the asymmetric stretch coordinate (dashed line). Excited-state potential energy surface parameters employed in this calculation are given in Table 2A. (B) Vibronic portion of the model absorption spectrum depicted in (A). (C) Comparison of the experimental absorption spectrum (solid line) to that calculated employing the three-dimensional ab initio potential (dashed line). Parameters for this calculation are given in Table 2B. (D) Vibronic portion of the model absorption spectrum depicted in (C).

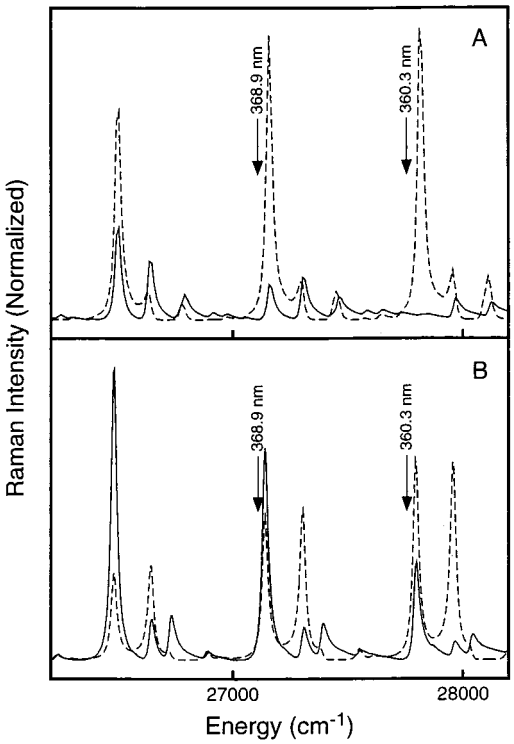

Figure 7. Resonance Raman excitation profiles of the symmetric stretch fundamental transition (solid line) and the asymmetric stretch overtone transition (dashed line) calculated using the double-well (A) and ab initio (B) surfaces. Parameters used in these calculations are provided in parts A and B of Table 2, respectively.

Resonance Raman. Figure 7 presents the resonance Raman excitation profiles for the symmetric stretch fundamental and asymmetric stretch overtone transitions calculated using the double-minimum and ab initio models. A quantitative comparison of these intensities to the experimental intensities is not presented for the following reasons. First, the calculation presented in Figure 7 is vibronic (i.e., rotational dynamics are not considered). Second, and more importantly, the uncertainty in the value of the homogeneous line width limits our ability to predict the absolute magnitude of the cross sections. Since resonance Raman cross sections are not normalized with respect to homogeneous broadening, an increase (decrease) in broadening would lead to a reduction (increase) in the predicted cross sections.[60−62] For the calculations presented in Figure 7, the homogeneous line width is 15 cm^{-1}, consistent with the absorption analysis presented above. It should also be noted that the homogeneous line width is level-dependent;[8] therefore, any treatment of homogeneous broadening in which level dependence is ignored is by definition qualitative.

Although the calculation of the resonance Raman cross sections is approximate, the results presented in Figure 7 illustrate the substantial spectroscopic differences that exist between the double-minimum and ab initio models. Both models predict that at certain excitation wavelengths, significant intensity should be observed for the asymmetric stretch overtone transition consistent with experiment. However, the predicted intensity of this transition relative to the symmetric stretch fundamental transition differs greatly between models. At 368.9 nm, the double-minimum model predicts that the asymmetric stretch overtone intensity should be substantial relative to the symmetric stretch fundamental, where the ab initio model predicts that these intensities should be comparable. Comparison to the experimental intensities (Figure 3) to these predictions suggests that the ab initio model provides a more accurate description of the $^2A_2$ surface. However, at 360.3 nm the double-minimum model predicts that the symmetric stretch fundamental should barely be observed, in agreement with experiment (Figure 3). Therefore, the experimental resonance Raman spectra obtained at this excitation wavelength appear to be consistent with the double-minimum model. In summary, the resonance Raman intensities demonstrate that significant evolution occurs along the asymmetric stretch following photoexcitation. The results presented in Figure 7 suggest that differentiation between models can be accomplished by monitoring the relative intensities of the asymmetric stretch overtone and symmetric stretch fundamental transitions as one varies the excitation wavelength systematically through a given vibronic transition. Such experiments are currently underway in an attempt to further characterize the curvature of the $^2A_2$ potential energy surface.

Discussion

Curvature of the $^2A_2$ Surface. The analysis of the absorption and resonance Raman intensities presented here demonstrates that following photoexcitation of gaseous OClO, significant excited-state structural relaxation occurs along all three normal coordinates. The $^2B_1-^2A_2$ absorption spectrum corresponds to a transition that involves Cl−O nonbonding to antibonding and O−O antibonding to bonding character resulting in an expected increase in Cl−O bond length and compression of the O−Cl−O bond angle.[82] Consistent with this expectation, the absorption spectrum (Figure 2) demonstrates vibronic progressions involv-

ing both symmetric coordinates. The resonance Raman intensities are consistent with excited-state structural evolution along these coordinates as well. In addition to evolution along the symmetric coordinates, substantial evolution along the asymmetric stretch coordinate occurs upon photoexcitation. The analysis of the room-temperature absorption spectrum presented above combined with the substantial resonance Raman intensity for the asymmetric stretch overtone transition (Figures 3 and 4) demonstrate conclusively that excited-state structural evolution occurs along this coordinate.

At issue is the nature of the $^2A_2$ surface along the asymmetric-stretch coordinate. The results presented here demonstrate that of the two existing models for this surface, the absorption intensities are better reproduced by the double-minimum model. It is important at this point to revisit the motivation for invoking the double-minimum model. The existence of a double-minimum along the asymmetric stretch coordinate for OClO has been proposed for some time. Mulliken originally suggested that for AB_2 systems, $1a_2$ to $2b_1$ electron promotion should initiate structural distortion to C_s symmetry in an attempt to minimize the antibonding character of the electron.[83] For example, the S_3 state of SO_2 is characterized by a double-minimum along the asymmetric stretch coordinate, presumably because of this effect.[84] Mulliken's suggestion was incorporated in the work of Coon and co-workers where a double-minimum potential was used to fit the anomalous absorption intensity of OClO for transitions involving the asymmetric stretch coordinate.[47] Richard and Vaida later refined these ideas and presented a potential that was capable of reproducing both the intensities and isotope splittings observed for absorption transitions involving the asymmetric stretch.[7]

Although the double-well potential is capable of modeling the absorption spectrum and a subset of the resonance Raman intensities, there are some aspects of the data that cannot be reproduced by this model. In particular, the weak asymmetric stretch fundamental intensity (1105 cm^{-1} in Figure 3) cannot be reproduced by the double-well model, since this potential is symmetric about $Q_3 = 0$. For SO_2, the gas-phase emission spectrum demonstrates asymmetric stretch fundamental activity, and Coriolis coupling has been proposed to explain this observation.[85] However, anharmonic coupling between the asymmetric stretch and either symmetric coordinate could asymmetrically distort the potential, resulting in fundamental intensity along this nominally nontotally symmetric coordinate.[86] It should be kept in mind that the asymmetric stretch fundamental intensity may be due to preresonant enhancement by states located in the VUV; however, preliminary excitation profiles obtained in our laboratory suggest that this is not the case. It is important to note that the ab initio surface does support the existence of anharmonic coupling between the symmetric and asymmetric stretch. Therefore, the observation of the asymmetric stretch fundamental intensity supports the ab initio model. In addition, it is difficult to ascertain why the substantial barrier along the asymmetric stretch predicted by the empirical double-minimum model is not reflected in the ab initio results, especially since ab initio calculations of SO_2 performed at a level comparable to the OClO calculations presented here are capable of reproducing the barrier on the S_3 surface.[87] The measured success of the ab initio surface in fitting the spectral features of OClO suggests a methodology by which an accurate description of the $^2A_2$ surface can be obtained. Specifically, a semiempirical model can be developed employing the ab initio surface as a starting point, with refinement of this surface accomplished by adjusting the potential until the spectroscopic properties of OClO are reproduced. This approach is currently being pursued.

Symmetry and OClO Photochemistry. The results presented here support the hypothesis that the symmetry established on the $^2A_2$ surface is important in defining the photoproduct formation dynamics. It has been suggested that in the gas phase, structural evolution along the asymmetric stretch potential results in the reduction of excited-state symmetry from C_{2v} to C_s.[1,10,57] This stands in contrast to the dynamics in solution where modest evolution occurs along this coordinate, and C_{2v} symmetry is preserved in the excited state.[28,32] Previous gas-phase experimental and theoretical work has suggested that a geometry at or near C_{2v} symmetry is a prerequisite for Cl formation. Recent ab initio results have indicated that the reduction of symmetry from C_{2v} to C_s serves to reduce the energy barrier for ClO and O formation.[57] In addition, only for geometries at or near C_{2v} symmetry was the production of Cl and O_2 predicted to be appreciable. This picture of OClO photoreactivity is supported by the recent studies of Davis and Lee where the production of Cl following photoexcitation of gaseous OClO was suggested to occur through a C_{2v} transition state.[10] In addition, it was demonstrated that excitation into transitions involving the asymmetric stretch coordinate resulted in a substantial reduction in Cl production. The combined experimental and theoretical results presented to date suggest that an excited-state geometry of C_{2v} symmetry is necessary for efficient Cl formation. Therefore, the environment dependence of the $^2A_2$ surface along the asymmetric stretch coordinate is potentially one component responsible for the phase dependence of Cl production.

Conclusions

In this paper, we have presented an analysis of the absorption and resonance Raman intensities of OClO. The first Raman spectra of gaseous OClO obtained directly on resonance with the $^2B_1 - ^2A_2$ transition were presented. Significant scattering intensity was observed for the symmetric stretch, bend, and asymmetric stretch, demonstrating that upon photoexcitation, structural evolution occurs along all three normal coordinates. The intensities of transitions involving the asymmetric stretch observed in the absorption and resonance Raman spectra were found to be consistent with the existence of a double-minimum along the asymmetric-stretch coordinate; however, the ab initio potential energy surface was also found to reproduce many of the major spectroscopic features. The results presented here support the emerging picture of OClO photochemistry where phase-dependent evolution along the asymmetric stretch coordinate serves to define the photochemical reactivity of this compound.

Acknowledgment. The National Science Foundation is acknowledged for their support of this work through the CAREER program (CHE-9701717 for P.J.R. and CHE-9501262 for K.A.P.). Acknowledgment is also made to the donors of the Petroleum Research Fund, administered by the American Chemical Society (P.J.R.). P.J.R. is a recipient of a Camille and Henry Dreyfus New Faculty Award and is a Cottrell Scholar of the Research Corporation.

References and Notes

(1) Vaida, V.; Simon, J. D. *Science* **1995**, *268*, 1443.
(2) Rowland, F. S. *Annu. Rev. Phys. Chem.* **1991**, *42*, 731.
(3) Burkholder, J. B.; Talukdar, R. K.; Ravishankara, A. R. *Geophys. Res. Lett.* **1994**, *21*, 585.
(4) Solomon, S.; Sanders, R. W.; Miller, H. L., Jr. *J. Geophys. Res.* **1990**, *95*, 13807.

(5) Sessler, J.; Chipperfield, M. P.; Pyle, J. A.; Toumi, R. *Geophys. Res. Lett.* **1995**, *22*, 687.
(6) Vaida, V.; Goudjil, K.; Simon, J. D.; Flanders, B. N. *J. Mol. Liq.* **1994**, *61*, 133.
(7) Richard, E. C.; Vaida, V. *J. Chem. Phys.* **1991**, *94*, 153.
(8) Richard, E. C.; Vaida, V. *J. Chem. Phys.* **1991**, *94*, 163.
(9) Vaida, V.; Solomon, S.; Richard, E. C.; Rühl, E.; Jefferson, A. *Nature* **1989**, *342*, 405.
(10) Davis, H. F.; Lee, Y. T. *J. Chem. Phys.* **1996**, *105*, 8142.
(11) Davis, H. F.; Lee, Y. T. *J. Phys. Chem.* **1992**, *96*, 5681.
(12) Bishenden, E.; Donaldson, D. J. *J. Chem. Phys.* **1994**, *101*, 9565.
(13) Bishenden, E.; Donaldson, D. J. *J. Chem. Phys.* **1993**, *99*, 3129.
(14) Bishenden, E.; Haddock, J.; Donaldson, D. J. *J. Phys. Chem.* **1991**, *95*, 2113.
(15) Chang, Y. J.; Simon, J. D. *J. Phys. Chem.* **1996**, *100*, 6406.
(16) Dunn, R. C.; Flanders, B. N.; Simon, J. D. *J. Phys. Chem.* **1995**, *99*, 7360.
(17) Dunn, R. C.; Anderson, J. L.; Foote, C. S.; Simon, J. D. *J. Am. Chem. Soc.* **1993**, *115*, 5307.
(18) Dunn, R. C.; Simon, J. D. *J. Am. Chem. Soc.* **1992**, *114*, 4856.
(19) Dunn, R. C.; Flanders, B. N.; Vaida, V.; Simon, J. D. *Spectrochim. Acta* **1992**, *48A*, 1293.
(20) Dunn, R. C.; Richard, E. C.; Vaida, V.; Simon, J. D. *J. Phys. Chem.* **1991**, *95*, 6060.
(21) Thøgersen, J.; Thomsen, C. L.; Poulsen, J. A.; Keiding, S. R. *J. Phys. Chem. A* **1998**, *102*, 4186.
(22) Poulsen, J. A.; Thomsen, C. L.; Keiding, S. R.; Thøgersen, J. *J. Chem. Phys.* **1998**, *108*, 8461.
(23) Thøgersen, J.; Jepsen, P. U.; Thomsen, C. L.; Poulsen, J. A.; Byberg, J. R.; Keiding, S. R. *J. Phys. Chem. A* **1997**, *101*, 3317.
(24) Liu, C.-P.; Lai, L.-H.; Lee, Y.-Y.; Hung, S.-C.; Lee, Y.-P. *J. Chem. Phys.* **1998**, *109*, 978.
(25) Lai, L.-H.; Liu, C.-P.; Lee, Y.-P. *J. Chem. Phys.* **1998**, *109*, 988.
(26) Furlan, A.; Scheld, H. A.; Huber, J. R. *J. Chem. Phys.* **1997**, *106*, 6538.
(27) Hayes, S. C.; Philpott, M. J.; Reid, P. J. *J. Chem. Phys.* **1998**, *109*, 2596.
(28) Foster, C. E.; Reid, P. J. *J. Phys. Chem. A* **1998**, *102*, 3541.
(29) Philpott, M. J.; Charalambous, S.; Reid, P. J. *Chem. Phys.* **1998**, *236*, 207.
(30) Philpott, M. J.; Charalambous, S.; Reid, P. J. *Chem. Phys. Lett.* **1997**, *281*, 1.
(31) Reid, P. J.; Esposito, A. P.; Foster, C. E.; Beckman, R. A. *J. Chem. Phys.* **1997**, *107*, 8262.
(32) Esposito, A.; Foster, C.; Beckman, R.; Reid, P. J. *J. Phys. Chem. A* **1997**, *101*, 5309.
(33) Gane, M. P.; Williams, N. A.; Sodeau, J. R. *J. Chem. Soc., Faraday Trans.* **1997**, *93*, 2747.
(34) Delmdahl, R. F.; Baumgartel, S.; Gericke, K.-H. *J. Chem. Phys.* **1996**, *194*, 2883.
(35) Burkholder, J. B.; Orlando, J. J.; Howard, C. J. *J. Phys. Chem.* **1990**, *94*, 687.
(36) Baumert, T.; Herek, J. L.; Zewail, A. H. *J. Chem. Phys.* **1993**, *99*, 4430.
(37) Lawrence, W. G.; Clemitshaw, K. C.; Apkarian, V. A. *J. Geophys. Res.* **1990**, *95*, 18591.
(38) Tanaka, K.; Tanaka, T. *J. Mol. Spectrosc.* **1983**, *98*, 425.
(39) Graham, J. D.; Roberts, J. T.; Brown, L. A.; Vaida, V. *J. Phys. Chem.* **1996**, *100*, 3115.
(40) Graham, J. D.; Roberts, J. T.; Anderson, L. D.; Grassian, V. H. *J. Phys. Chem.* **1996**, *100*, 19551.
(41) Brown, L. A.; Vaida, V.; Hanson, D. R.; Graham, J. D.; Roberts, J. T. *J. Phys. Chem.* **1996**, *100*, 3121.
(42) Flesch, R.; Wassermann, B.; Rothmund, B.; Rühl, E. *J. Phys. Chem.* **1994**, *98*, 6263.
(43) Rühl, E.; Jefferson, A.; Vaida, V. *J. Phys. Chem.* **1990**, *94*, 2990.
(44) Hamada, Y.; Merer, A. J.; Michielsen, S.; Rice, S. A. *J. Mol. Spectrosc.* **1981**, *86*, 499.
(45) McDonald, P. A.; Innes, K. K. *Chem. Phys. Lett.* **1978**, *59*, 562.
(46) Brand, J. C. D.; Redding, R. W.; Richardson, A. W. *J. Mol. Spectrosc.* **1970**, *34*, 399.
(47) Coon, J. B. *J. Chem. Phys.* **1946**, *14*, 665.
(48) Coon, J. B. *Phys. Rev.* **1940**, *58*, 926.
(49) Müller, H. S. P.; Willner, H. *J. Phys. Chem.* **1993**, *97*, 10589.
(50) Lanzendorf, E. J.; Kummel, A. C. *Geophys. Res. Lett.* **1996**, *23*, 1251.
(51) Pursell, C. J.; Conyers, J.; Alapat, P.; Parveen, R. *J. Phys. Chem.* **1995**, *99*, 10433.
(52) Adrian, F. J.; Bohandy, J.; Kim, B. F. *J. Chem. Phys.* **1986**, *85*, 2692.
(53) Arkell, A.; Schwager, I. *J. Am. Chem. Soc.* **1967**, *89*, 5999.
(54) Rochkind, M. M.; Pimentel, G. C. *J. Chem. Phys.* **1967**, *46*, 4481.
(55) Gole, J. L. *J. Phys. Chem.* **1980**, *84*, 1333.
(56) Peterson, K. A. *J. Chem. Phys.* **1998**, *109*, 8864.
(57) Peterson, K. A.; Werner, H.-J. *J. Chem. Phys.* **1996**, *105*, 9823.
(58) Peterson, K. A.; Werner, H.-J. *J. Chem. Phys.* **1992**, *96*, 8948.
(59) Johnsson, K.; Engdahl, A.; Ouis, P.; Nelander, B. *J. Mol. Struct.* **1993**, *293*, 137.
(60) Myers, A. B. *J. Raman Spectrosc.* **1997**, *28*, 389.
(61) Myers, A. B.; Li, B. *J. Chem. Phys.* **1990**, *92*, 3310.
(62) Myers, A. B.; Mathies, R. A. Resonance Raman Intensities: A Probe of Excited State Structure and Dynamics. In *Biological Applications of Raman Spectroscopy: Resonance Raman Spectra of Polyenes and Aromatics*; Spiro, T. G., Ed.; John Wiley & Sons: New York, 1987; Vol. 2, pp 1−58.
(63) Mauldin, R. L., III; Burkholder, J. B.; Ravishankara, A. R. *J. Phys. Chem.* **1992**, *96*, 2582.
(64) Lee, S.-Y.; Heller, E. J. *J. Chem. Phys.* **1979**, *71*, 4777.
(65) Tannor, D. J.; Heller, E. J. *J. Chem. Phys.* **1982**, *77*, 202.
(66) Allen, H. C. J.; Cross, P. C. *Molecular Vib-Rotors: The Theory and Interpretation of High Resolution Infrared Spectra*; John Wiley and Sons: New York, 1963.
(67) Papoušek, D.; Aliev, M. R. *Molecular Vibrational−Rotational Spectra*; Elsevier Scientific Publishing Co.: Amsterdam, 1982; Vol. 17.
(68) Kroto, H. W. *Molecular Rotation Spectra*; John Wiley and Sons, Ltd.: London, 1975.
(69) Zare, R. N. *Angular Momentum: Understanding Spatial Aspects in Chemistry and Physics*; Wiley: New York, 1988.
(70) Li, B.; Myers, A. B. *J. Chem. Phys.* **1991**, *94*, 2458.
(71) Ziegler, L. D. *J. Chem. Phys.* **1987**, *87*, 4498.
(72) Sue, J.; Yan, Y. J.; Mukamel, S. *J. Chem. Phys.* **1986**, *85*, 462.
(73) Feit, M. D.; Fleck, J. A. *J. Chem. Phys.* **1983**, *78*, 301.
(74) Feit, M. D.; Fleck, J. A.; Steiger, A. *J. Comput. Phys.* **1982**, *47*, 412.
(75) Califano, S. *Vibrational States*; John Wiley & Sons: London, 1976.
(76) Truong, T. N.; Tanner, J. J.; Bala, P.; McCammon, J. A.; Kouri, D. J.; Lesyng, B.; Hoffman, D. K. *J. Chem. Phys.* **1992**, *96*, 2077.
(77) Ziegler, L. D. *Acc. Chem. Res.* **1994**, *27*, 1.
(78) Richardson, A. W.; Redding, R. W.; Brand, J. C. D. *J. Mol. Spectrosc.* **1969**, *29*, 93.
(79) Lawless, M. K.; Reid, P. J.; Mathies, R. A. Analysis of Condensed Phase Photochemical Reaction Mechanisms with Resonance Raman Spectroscopy. In *Ultrafast Dynamics of Chemical Systems*; Simon, J. D., Ed.; Kluwer: Amsterdam, 1994; pp 267−287.
(80) Karplus, M.; Porter, R. N. *Atoms and Molecules*; W. A. Benjamin, Inc.: New York, 1970.
(81) Chi, F. K.; Andrews, L. *J. Mol. Spectrosc.* **1974**, *52*, 82.
(82) Walsh, A. D. *J. Chem. Soc.* **1953**, 2266.
(83) Mulliken, R. A. *Can. J. Chem.* **1958**, *36*, 10.
(84) Hoy, A. R.; Brand, J. C. D. *Mol. Phys.* **1978**, *36*, 1409.
(85) Brand, J. C. D.; Humphrey, D. R.; Douglas, A. E.; Zanon, I. *Can. J. Phys.* **1973**, *51*, 530.
(86) Yang, T.-S.; Myers, A. B. *J. Chem. Phys.* **1991**, *95*, 6207.
(87) Peterson, K. A. Unpublished results.